Supporting information:

Combined effect of germanium doping and grain alignment on oxide-ion conductivity of apatite-type lanthanum silicate polycrystal

Koichiro Fukuda,[*,†] Toru Asaka,[†] Nobuo Ishizawa,[†] Hiroki Mino,[†] Daisuke Urushihara,[†] Abid Berghout,[‡] Emilie Béchade,[‡] Olivier Masson,[‡] Isabelle Julien,[‡] and Philippe Thomas[‡]

[†]Department of Environmental and Materials Engineering, Nagoya Institute of Technology, Nagoya 466-8555, Japan

[‡]Science des Procédés Céramiques et de Traitements de Surface - SPCTS, UMR 6638, Centre Européen de la Céramique, 12 Rue Atlantis, 87068 Limoges Cedex, France

Table S1 Summary of data collection and refinement parameters

Chemical composition	$La_{9.93}Si_{5.23(1)}Ge_{0.77(1)}O_{26}$
Space group	$P6_3/m$ (No. 176)
a / nm	0.97508(2)
c / nm	0.72153(1)
V / nm^3	0.59411(2)
Z	1
Formula weight	1914.7
D_x / Mgm^{-3}	5.352
F(000)	837.6
μ / mm^{-1}	17.69
Temperature / K	293
Crystal color	clear
Crystal form	rectangular
Crystal size / μm	approximately 15 × 10 × 10
No. of observed reflections	21510
$R[F^2 > 3\sigma(F^2)]$	0.0121
$wR(F^2)$	0.0183
S	1.35
No. of unique reflections $[F^2 > 3\sigma(F^2)]$	1567
Collection range	$-19 \le h \le 16$ $-19 \le k \le 19$ $-14 \le l \le 14$

Table S2 Fitted parameters after deconvolution in the 750 cm^{-1} – 950 cm^{-1} spectral range

Sample	Band wavenumber / cm^{-1}	Normalized Intensity	Full-width at half-maximum / cm^{-1}	Gaussian/Lorentzian ratio
Apatite sublayer I	789	1	28.7	1
	845	4.41	18.2	0.75
	854	4.81	19.2	0.47
	869	1.71	21.7	0.63
$La_{9.33}(Si_{0.9}Ge_{0.1})_6O_{26}$	794	1	25.3	1
	845	1.79	16.8	0.57
	854	1.46	17.1	0.33
	866	0.60	22.2	0.32
$La_{9.33}(Si_{0.85}Ge_{0.15})_6O_{26}$	795	1	26.7	0.31
	845	0.79	17.8	0.62
	853	0.88	17.3	0.68
	867	0.18	21.1	0.41
$La_{9.33}(Si_{0.8}Ge_{0.2})_6O_{26}$	794	1	28.3	0.07
	844	2.54	18.3	0.69
	852	2.57	20.8	1
	870	0.44	20.3	1.00

Table S3 Anharmonic atomic displacement parameters from the 3rd order to the 4th order of La1 and La2 sites

La1

3rd order (×10 nm^3)

C_{111}	C_{112}	C_{113}	C_{122}	C_{123}	C_{133}	C_{222}	C_{223}
-0.00023(2)	-0.00037(2)	-0.00055(2)	C_{112}-C_{111}	1/2 C_{113}	0	-C_{111}	C_{113}
C_{233}	C_{333}						
0	-0.00111(9)						

4th order (×10^3 nm^3)

D_{1111}	D_{1112}	D_{1113}	D_{1122}	D_{1123}	D_{1133}	D_{1222}	D_{1223}
0.00034(3)	1/2 D_{1111}	-0.000008(10)	1/2 D_{1111}	-0.000003(10)	0.00009(2)	1/2 D_{1111}	D_{1123}-D_{1113}
D_{1233}	D_{1333}	D_{2222}	D_{2223}	D_{2233}	D_{2333}	D_{3333}	
1/2 D_{1133}	0	D_{1111}	-D_{1113}	D_{1133}	0	0.00160(11)	

La2

3rd order (×10 nm^3)

C_{111}	C_{112}	C_{113}	C_{122}	C_{123}	C_{133}	C_{222}	C_{223}
0.00018(3)	0.00003(2)	0	0.00000(2)	0	0.00017(2)	-0.00009(3)	0
C_{233}	C_{333}						
-0.00004(2)	0						

4th order (×10^3 nm^3)

D_{1111}	D_{1112}	D_{1113}	D_{1122}	D_{1123}	D_{1133}	D_{1222}	D_{1223}
0.00005(2)	0.000019(14)	0	0.000027(13)	0	0.000148(12)	0.000031(14)	0
D_{1233}	D_{1333}	D_{2222}	D_{2223}	D_{2233}	D_{2333}	D_{3333}	
0.000066(8)	0	0.00008(3)	0	0.000175(12)	0	0.00035(5)	

Table S4 Selected interatomic distances (nm) for $La_{9.93}(Si_{0.87}Ge_{0.13})_6O_{26}$

La1–O1	0.25451(13) × 3
La1–O2	0.24859(13) × 3
La1–O3A	0.3255(7) × 3 × *g*(O3A)
La1–O3B	0.2798(2) × 3 × *g*(O3B)
<La1–O>	0.2645
La2–O1	0.25172(13)
La2–O2	0.2768(2)
La2–O3A	0.2501(6) × 2 × *g*(O3A)
La2–O3B	0.2475(2) × 2 × *g*(O3B)
La2–O3A^{i}	0.2516(6) × 2 × *g*(O3A)
La2–O3B^{i}	0.2631(2) × 2 × *g*(O3B)
La2–O4	0.23103(3)
<La2–O>	0.2538
Si/Ge–O1	0.16441(13)
Si/Ge–O2	0.1630(2)
Si/Ge–O3A	0.1625(5) × 2 × *g*(O3A)
Si/Ge–O3B	0.1660(2) × 2 × *g*(O3B)
<Si/Ge–O>	0.1645

Symmetry code: (i) $x-y, x, -z$.
Site occupancies (*g*) of O3A and O3B given in Table 1.

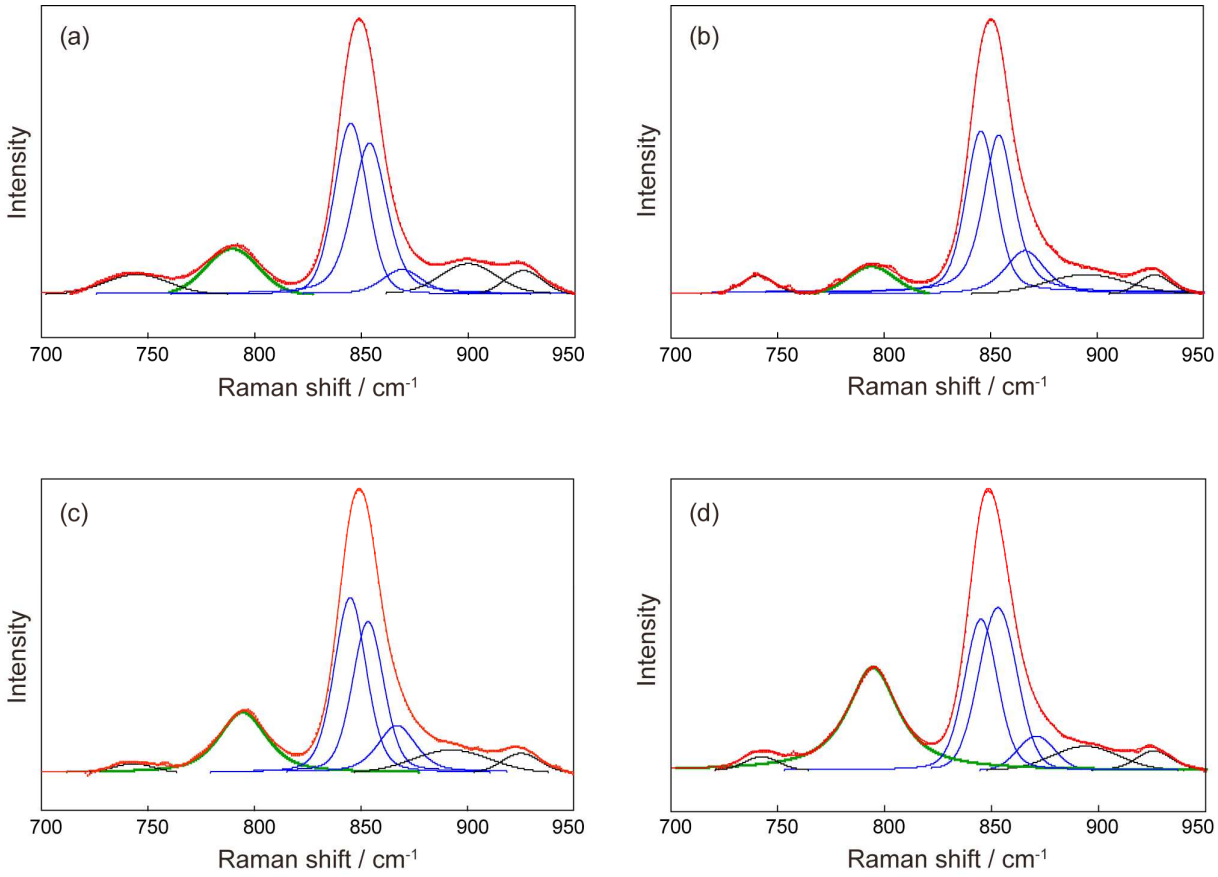

Figure S1. Mixed Gaussian/Lorentzian deconvolution of the Raman spectra of (a) the apatite sublayer I and the standard specimens of (b) $La_{9.33}(Si_{0.9}Ge_{0.1})_6O_{26}$ (c) $La_{9.33}(Si_{0.85}Ge_{0.15})_6O_{26}$ and (d) $La_{9.33}(Si_{0.8}Ge_{0.2})_6O_{26}$. The overlapping bands in these spectra, ranging from 700 cm^{-1} to 950 cm^{-1}, were deconvoluted by fitting them to Gaussian/Lorentzian band shapes, after subtraction of the baselines. The intense band of ca. 850 cm^{-1} in each spectrum is composed of the three bands of ca. 847, 856 and 866 cm^{-1}. The band wavenumber positions, band intensities, full-widths at half-maximum and Gaussian/Lorentzian ratios are summarized in Table S2, in which the band intensities are normalized to unity for the first band in each spectrum.

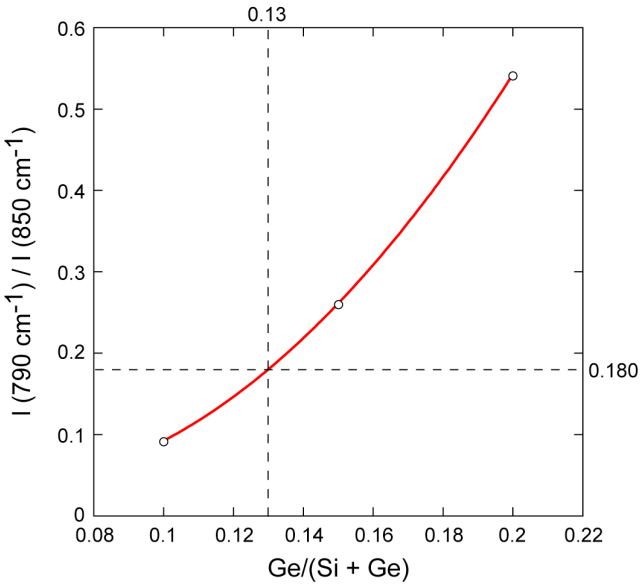

Figure S2. Plot of the ratio of the intensity of the strong band at ca. 850 cm^{-1} to the weak band at ca.790 cm^{-1} versus the Ge content. The intensity of the former band, I (850 cm^{-1}), is determined from the summation of the extracted intensities for the three components at ca. 847, 856 and 866 cm^{-1}; I (850 cm^{-1}) = I (847 cm^{-1}) + I (856 cm^{-1}) + I (866 cm^{-1}). The Ge/(Si + Ge) ratio of the apatite sublayer I is determined to be Ge/(Si + Ge) = 0.13 from I (790 cm^{-1})/I (850 cm^{-1}) = 0.180.

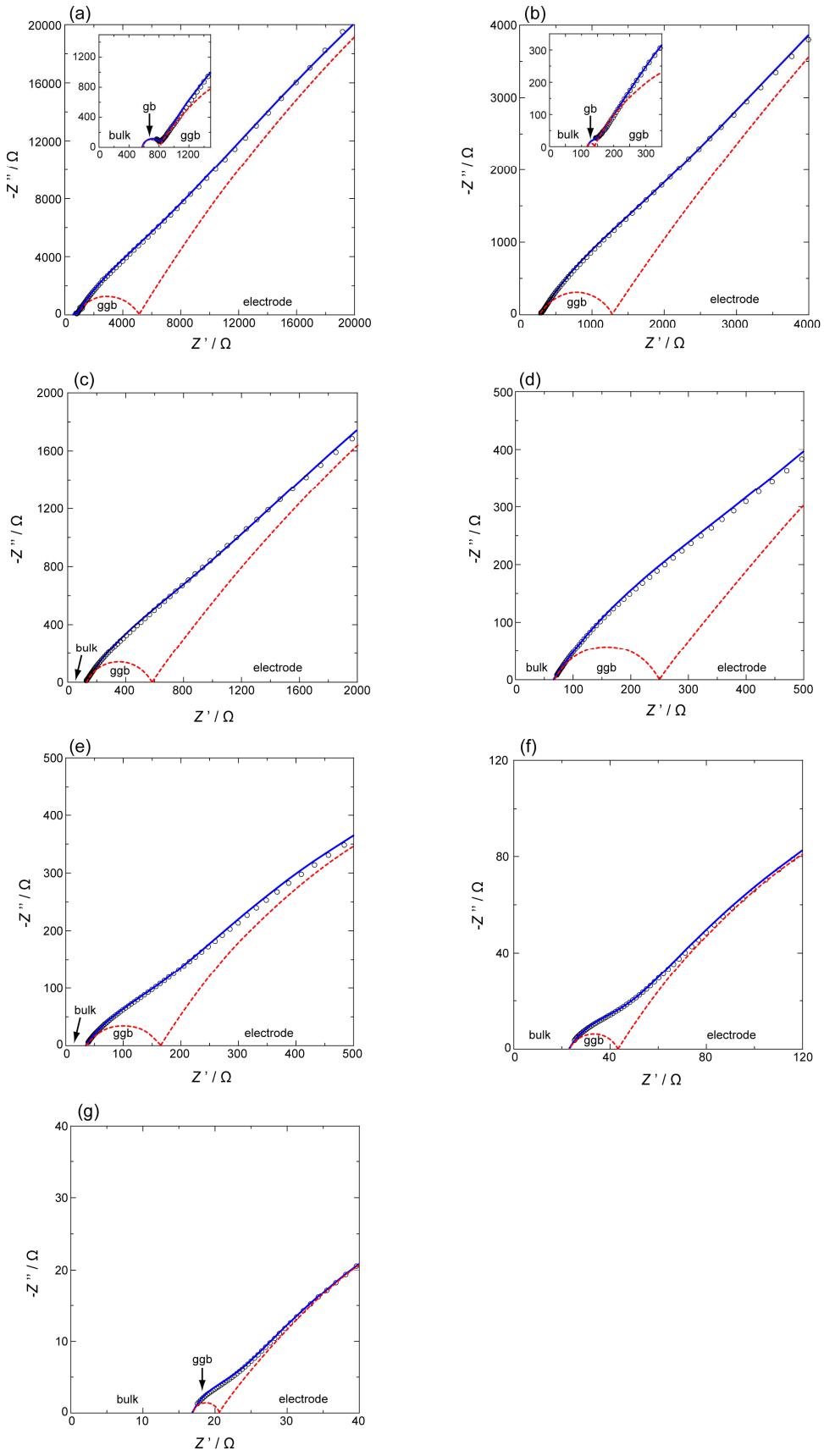

Figure S3. A series of Nyquist plots of the $La_{9.33}(Si_{0.87}Ge_{0.13})_6O_{26}$ polycrystalline electrolyte. Data collected at (a) 673 K, (b) 723 K, (c) 773 K, (d) 823 K, (e) 873 K, (f) 923 K and (g) 973 K.

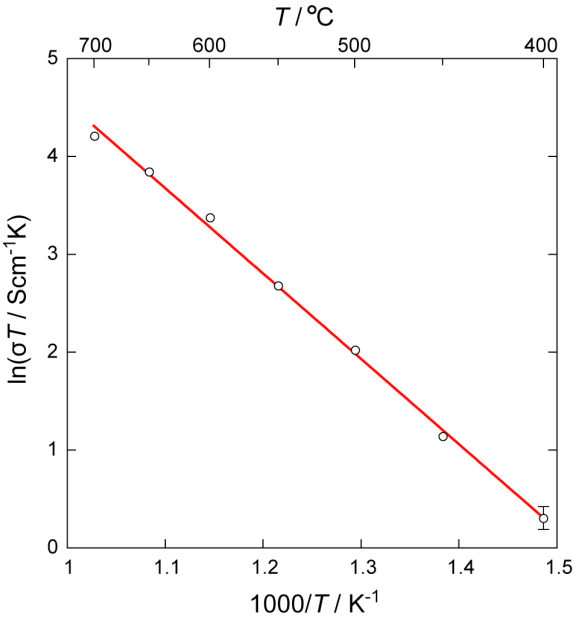

Figure S4. Arrhenius plot of the bulk conductivity almost along the *c*-axis for $La_{9.33}(Si_{0.87}Ge_{0.13})_6O_{26}$.